# Early Synaptic Defects in *tulp1*−/− Mice

**Gregory H. Grossman**[1], **Gayle J. T. Pauer**[1], **Umadevi Narendra**[1], **Neal S. Peachey**[1,2,3], and **Stephanie A. Hagstrom**[1,3]

[1]Department of Ophthalmic Research, Cole Eye Institute, Cleveland Clinic, Cleveland, Ohio

[2]Research Service, Cleveland Veterans Administration Medical Center, Cleveland, Ohio

[3]Department of Ophthalmology, Cleveland Clinic Lerner College of Medicine, Case Western Reserve University, Cleveland, Ohio

## Abstract

**PURPOSE**—Mutations in the photoreceptor-specific tubby-like protein 1 (*TULP1*) underlie a form of autosomal recessive retinitis pigmentosa. To investigate the role of Tulp1 in the photoreceptor synapse, the authors examined the presynaptic and postsynaptic architecture and retinal function in *tulp1*−/− mice

**METHODS**—The authors used immunohistochemistry to examine *tulp1*−/− mice before retinal degeneration and made comparisons with wild-type (wt) littermates and retinal degeneration 10 (rd10) mice, another model of photoreceptor degeneration that has a comparable rate of degeneration. Retinal function was characterized with the use of electroretinography.

**RESULTS**—In wt mice, Tulp1 is localized to the photoreceptor synapse. In the *tulp1*−/− synapse, the spatial relationship between the ribbon-associated proteins Bassoon and Piccolo are disrupted, and few intact ribbons are present. Furthermore, bipolar cell dendrites are stunted. Comparable abnormalities are not seen in rd10 mice. The leading edge of the a-wave had normal kinetics in *tulp1*−/− mice but reduced gain in rd10 mice. The b-wave intensity-response functions of *tulp1*−/− mice are shifted to higher intensities than in wt mice, but those of rd10 mice are not.

**CONCLUSIONS**—Photoreceptor synapses and bipolar cell dendrites in *tulp1*−/− mice display abnormal structure and function. A malformation of the photoreceptor synaptic ribbon is likely the cause of the dystrophy in bipolar cell dendrites. The association of early-onset, severe photoreceptor degeneration preceded by synaptic abnormalities appears to represent a phenotype not previously described. Not only is Tulp1 critical for photoreceptor function and survival, it is essential for the proper development of the photoreceptor synapse.

The outer plexiform layer (OPL) of the vertebrate retina is where rod and cone photoreceptors make synaptic contact with second-order neurons of the inner nuclear layer (INL).[1] Photoreceptors signal second-order neurons with the use of a graded synaptic output, whereby changes in stimulus intensity are conveyed by alterations in the tonic release of neurotransmitter at the active zone of the photoreceptor presynaptic membrane.[1] In addition to this tonic release, the visual sensory system requires rapid transfer of information.[2] At the photoreceptor synapse, hundreds of neurotransmitter-laden vesicles come in contact with the presynaptic membrane every second, liberating glutamate into the synaptic cleft. To support these requirements, photoreceptor terminals contain a highly

Corresponding author: Stephanie A. Hagstrom, Department of Ophthalmic Research, Cole Eye Institute, Cleveland Clinic, 9500 Euclid Avenue, Cleveland, OH 44195; hagstrs@ccf.org.

specialized presynaptic apparatus, the ribbon synapse, which is thought to be a critical platform for the rapid transport, tethering, docking, and recycling of synaptic vesicles.[1,3]

Rod photoreceptor terminals typically contain a single ribbon, whereas larger cone terminals harbor multiple ribbons.[1] Although many of the structural elements have been examined, the complete complement of their elements and how they interact to form functional synapses remain elusive. More insight into photoreceptor synaptic function is necessary for thorough understanding of the many disorders that affect vision.[2,4]

Retinitis pigmentosa (RP) refers to a large number of inherited retinal disorders characterized by photoreceptor degeneration. RP, which is genetically and phenotypically heterogeneous, affects more than 1 million persons worldwide.[5,6] Mutations in *TULP1* underlie an early-onset, severe form of autosomal recessive RP.[7–10] TULP1 is a member of the Tubby-like protein family, which includes TULP2, TULP3, and TUB.[11] TUB and TULP3 are widely distributed throughout the central nervous system; expression of TULP1 and TULP2 is restricted largely to rod and cone photoreceptors and the testis, respectively. [11–16] Although the complete role of TULPs in the central nervous system remains unclear, TULP proteins are known to play important roles in neuronal development and function. This is emphasized by the association of *TUB* and *TULP1* mutations with neurosensory disease phenotypes.[7–10,12,17]

Tulp1 is expressed exclusively in photoreceptors, localizing to the inner segment (IS), connecting cilium, perikarya, and terminals.[18–20] Although the function of Tulp1 remains elusive, there is evidence that Tulp1 plays a role in intracellular trafficking in the IS and at the photoreceptor synapse.[18,20–22] Tulp1 is a cytoplasmic protein that associates with cellular membranes and the actin cytoskeleton.[21] In *tulp1*$^{-/-}$ mice, photoreceptor cells degenerate, rod and cone opsins are mislocalized, and rhodopsin-bearing extracellular vesicles accumulate around the ellipsoid region of the IS.[18] These defects indicate that Tulp1 may be involved in actin cytoskeletal dynamics such as protein transport from the IS to the outer segment (OS) through the connecting cilium.[18,20–22]

We recently showed that Tulp1 colocalizes with and binds to the neuronal-specific protein Dynamin-1 at the IS and the terminals of photoreceptors.[22] Dynamin-1 is a GTPase that binds actin and regulates endocytosis, vesicle development, and movement at the trans-Golgi network, the plasma membrane, and the synaptic membrane.[22–24] Consistent with a role for Tulp1 at the photoreceptor synapse, the b-wave component of the electroretinogram (ERG) generated by depolarizing bipolar cells (DBCs) is markedly reduced in young *tulp1*$^{-/-}$ mice.[22]

These results suggest that Tulp1 plays an important role in synaptic function and motivated us to look more closely at the photoreceptor synapse. To accomplish this, we examined the architecture of the *tulp1*$^{-/-}$ synapse at postnatal day (P)16, an age at which synaptic development is complete in wild-type (wt) mice[25] and precedes photoreceptor degeneration in *tulp1*$^{-/-}$ mice.[18] To ascertain whether alterations are specific to the *tulp1*$^{-/-}$ retina and are not merely a consequence of the degenerative process, we made parallel studies of the retinal degeneration 10 (rd10) mouse, which experiences a comparable rate of photoreceptor degeneration because of a point mutation in exon 13 of the β-subunit of the rod cGMP phosphodiesterase gene.[26] Except for the comparable rate of degeneration, no reports have been published of early synaptic abnormalities associated with this model; thus, it presents a fitting control strain for synaptic-specific comparisons. Although mouse models with synaptic-specific mutations (such as *Cabp4*$^{-/-}$,[27] *Cacna1f*$^{nob2}$,[28] and *Bsn*$^{-/-}$[29]) exhibit decreased b-waves, altered bipolar dendrites, and presynaptic abnormalities, they do not

exhibit photoreceptor degeneration or rhodopsin mislocalization comparable to that observed in *tulp1*$^{-/-}$ mice.

In this study, we verified that Tulp1 is diffusely localized to the photoreceptor synapse and that its distribution overlaps that of several key synaptic proteins. Mice deficient in Tulp1 lack the tight spatial relationship between the ribbon-associated proteins, Bassoon and Piccolo, characteristic of wt animals. In addition, few intact ribbons are present in the OPL. We also report that dendrites of second-order neurons exhibit abnormalities at an early age in *tulp1*$^{-/-}$ mice. These structural defects are not apparent in rd10 animals. Although ERG a-waves of *tulp1*$^{-/-}$ mice are reduced in amplitude, they retain normal kinetics. In comparison, the *tulp1*$^{-/-}$ b-wave intensity-response function is desensitized, consistent with a functional defect at the photoreceptor output synapse. That similar synaptic and b-wave changes were not seen in rd10 mice indicates they are not generalized responses to photoreceptor degeneration. These results indicate that the absence of Tulp1 is associated with a synaptic malformation that precedes photoreceptor degeneration and most likely interferes with the proper development of postreceptoral neurons. Taken together, this appears to represent a phenotype not previously described. These data indicate that Tulp1 plays an important role in photoreceptor synapse development and in photoreceptor function and survival.

## METHODS

### Animals

The generation of *tulp1*$^{-/-}$ mice has been described previously and is now maintained on a C57BL/6 background.[18] Mice studied here were derived from mating *tulp1*$^{+/-}$ heterozygotes and were genotyped by PCR amplification of genomic DNA, as previously described.[18] Homozygous rd10 breeders (B6.CXB1-*Pde6b*$^{RD10}$/J) were purchased from The Jackson Laboratory (Bar Harbor, ME). Mice were euthanatized by $CO_2$ inhalation or by drug overdose; cervical dislocation followed. All experiments on animals were approved by the Institutional Animal Care and Use Committee of the Cleveland Clinic and were performed in compliance with the ARVO Statement for the Use of Animals in Ophthalmic and Visual Research.

### Preparation of Retinal Sections

Mouse eyes were prepared as previously described.[22] Briefly, eyes were fixed in 4% paraformaldehyde in PBS for 60 minutes. After removal of the cornea and lens, the posterior pole was immersed through a graded series of sucrose solutions as follows: 10% for 1 hour, 20% for 1 hour, and 30% overnight. The posterior pole was embedded in OCT freezing medium, flash frozen on powderized dry ice, and immediately transferred to −80°C. Tissue was sectioned at 10-µm thickness with a cryostat (Leica, Wetzlar, Germany) at −30°C.

### Immunofluorescence Staining

Retinal sections were blocked in 5% bovine serum albumin and 1% normal goat serum with 0.1% Triton X-100 for 1 hour before incubation with primary antibodies overnight at 4°C. Primary antibodies and dilutions were as follows: Tulp1, rabbit polyclonal M-tulp1N 1:250[20]; Piccolo, rabbit polyclonal 1:500 (ab20664; Abcam Inc., Cambridge, MA); Bassoon, mouse monoclonal 1:500 (SAP7F407; Assay Designs Inc., Ann Arbor, MI); Ribeye/CtBP2, mouse monoclonal 1:500 (612044; BD Biosciences, San Jose, CA); protein kinase C-α (PKC), rabbit polyclonal 1:1000 (SC208; Santa Cruz Biotechnology Inc., Santa Cruz, CA); rhodopsin, mouse monoclonal 1:100 (B630N; Paul Hargrave, University of Florida, Gainesville, FL). After three washes in PBS, sections were incubated in fluorescent secondary antibodies at room temperature for 1 hour. Secondary antibodies were Alexa

Fluor 488 goat anti–rabbit IgG and goat anti–mouse IgG and Alexa Fluor 594 goat anti–rabbit IgG and goat anti–mouse IgG (Invitrogen, Carlsbad, CA). Sections were then rinsed three times in PBS and then rinsed lightly in dH$_2$O and were coverslipped with mounting medium with DAPI (Vectashield; Vector Laboratories, Burlingame, CA). Sections were imaged with a fluorescence microscope (BX-61; Olympus, Tokyo, Japan) equipped with a charge-coupled device monochrome camera (Hamamatsu Photonics, Bridgewater, NJ). For the imaging of ribbon-associated synaptic proteins (Bassoon, Piccolo, and Ribeye), 2-µm Z-stacks were acquired with nearest-neighbor deconvolution, followed by a maximum intensity Z-axis projection (SlideBook software, version 4.2; Intelligent Imaging Innovations, Denver, CO).

## Electroretinography

ERGs were recorded from *tulp1$^{-/-}$*, *tulp1$^{+/-}$*, and wt littermates and from rd10 homozygotes at P16. After overnight dark adaptation, mice were anesthetized with ketamine (80 mg/kg) and xylazine (16 mg/kg). Eyedrops were used to anesthetize the cornea (1% proparacaine HCl) and to dilate the pupil (1% mydriacyl, 2.5% phenylephrine HCl, 1% cyclopentolate HCl). Mice were placed on a temperature-regulated heating pad throughout the recording session. ERGs were recorded with a stainless steel electrode that made contact with the corneal surface through a thin layer of 0.7% methylcellulose. Needle electrodes placed in the cheek and the tail served as reference and ground leads, respectively. Responses were differentially amplified (0.3–1500 Hz), averaged, and stored with the use of a signal averaging system (UTAS E-3000; LKC Technologies, Gaithersburg, MD). ERGs were recorded to flash stimuli presented in an LKC Technologies ganzfeld that ranged in intensity from −3.6 to 2.1 log cd · s/m$^2$.

Amplitude of the a-wave was measured at 8 ms after flash presentation from the prestimulus baseline. Amplitude of the b-wave was measured from the a-wave trough to the peak of the b-wave or, if no a-wave was present, from the prestimulus baseline. Implicit time of the b-wave was measured from the time of flash presentation to the b-wave peak.

The b-wave intensity-response function was analyzed using equation (1)

$$R/R_{max} = I^n/(I^n + K^n)$$

(1)

in which *R* represents the b-wave obtained to background intensity *I*, $R_{max}$ represents the amplitude asymptote, *K* represents the flash intensity required to generate a b-wave response that is ½ of $R_{max}$, and *n* is a dimensionless slope parameter. As in humans, the b-wave intensity-response function in mice includes a high-intensity limb where the a-wave begins to precede the b-wave.[30] We fit equation 1 only to data points that fell below this second limb.

We analyzed the leading edge of the dark-adapted a-waves obtained to high-intensity stimuli in terms of a modified form of the Lamb and Pugh model of rod phototransduction[31,32]

$$P3(i,t) = \{1 - \exp[-iA(t - td)2]\}RmP3$$

(2)

in which *P3* represents the mass response of the rod photoreceptors, the amplitude of which is expressed as a function of flash energy (*i*) and time (*t*) after flash onset, *A* represents the gain of phototransduction, *RmP3* represents the maximum response, and *td* represents a brief delay.

### Dendritic Field Analysis

Four PKC immunoreactive retinas from each genotype (*tulp1*^{−/−}, wt, and rd10) were imaged under an fluorescence microscope (BX-60; Olympus). For analysis, individual images were imported into a program (Image-Pro PLUS, version 6.2; Media Cybernetics, Inc., Bethesda, MD) that measured the PKC immunoreactive dendrites. Only the portions of the dendrites that extended beyond the cell bodies of the bipolar cells of INL were measured (nuclei were verified by DAPI staining). Dendrite lengths were measured over the entire area of the images (213 µm × 162 µm). Two images were taken from the superior or the inferior retina of each animal; one was taken from the central retina (within 200 µm of the optic nerve) or the peripheral retina (within 200 µm of the peripheral edge). Measurements were averaged per genotype and were reported as having been derived from the central or peripheral retina.

## RESULTS

### Photoreceptor Synaptic Localization of Tulp1

The retinal distribution of Tulp1 was examined in wt mouse sections at P16 (Fig. 1A). Consistent with previous observations, Tulp1 staining is strongest in the IS and OPL but is absent in the OS.[18−20] Staining in the outer nuclear layer (ONL) appeared to be located in the perikarya and did not overlap with the nuclei. Tulp1 staining in the OPL was diffuse and appeared to fill the entire terminal, and its colocalization with the presynaptic ribbon-associated protein Bassoon confirmed its presence in the photoreceptor synapse (Fig. 1B).

### Malformation of *tulp1*^{−/−} Photoreceptor Synapses

To characterize synaptic terminal architecture of *tulp1*^{−/−} mice, we examined the distribution of synaptic proteins at ages before photoreceptor degeneration. Piccolo and Bassoon proteins have been implicated in the organization of the photoreceptor synapse, the functioning of the ribbon, and the trafficking of vesicles at the synapse.[25,33] These proteins normally localize together at the presynaptic membrane with a horseshoe-like spatial arrangement.[25,33] Figure 2A shows a wt mouse retinal section at P16 double-stained with antibodies to Piccolo (red) and Bassoon (green). Arrows highlight examples of the normal steric relationship between these two ribbon-associated proteins. A profoundly different appearance was noted in *tulp1*^{−/−} mice at the same age, when the structure and distribution of both Piccolo and Bassoon were markedly abnormal (Fig. 2B). In contrast to the horseshoe-shaped ribbons typical of wt mice, Bassoon and Piccolo staining in the *tulp1*^{−/−} retina appeared punctate, and normal ribbons were rarely seen. Moreover, even though the two proteins were in proximity, few terminals displayed any coupling between Piccolo and Bassoon. To determine whether these abnormalities were secondary to an early degenerative process, we also examined the rd10 mouse model in which the onset of degeneration occurred between P16 and P18,[34,35] similar to that of *tulp1*^{−/−} mice[18] but caused by a different molecular defect. As shown in Figure 2C, Piccolo and Bassoon were normally aligned in the photoreceptor terminals of rd10 mice at P16. Moreover, this relationship was preserved at P21, an age when photoreceptor cell death is maximal (Fig. 2D), suggesting that the synaptic abnormalities in the *tulp1*^{−/−} retina are not secondary to an early degenerative process.[34,35]

To examine more closely the coupling of Bassoon and Piccolo at P16, we generated three-dimensional surface plots from deconvoluted 2-µm Z-axis stacks of immunofluorescent images of wt and *tulp1*^{−/−} OPLs (Figs. 2E, F). Deconvolution microscopy significantly reduces the blurring effect of reflected and emitted light associated with sources above or below a focal plane of interest. This results in images with increased resolution and markedly improved contrast, thus revealing structural information normally obscured in images generated by traditional methods.[36] Implementing three-dimensional surface volume

reconstruction then allows the viewing of relationships between objects in a three-dimensional landscape, further revealing associations normally not detected in two-dimensional microscopy. This analysis shows that Bassoon and Piccolo are often in immediate proximity with one another in the *tulp1*^{−/−} retina (Fig. 2F; arrowheads indicate independent ribbon staining) but confirms that they are rarely spatially aligned into the normal horseshoe-shaped ribbon architecture typical of wt mice (Fig. 2E; arrows indicate coupling).

To examine whether normal terminal architecture is ever present in *tulp1*^{−/−} mice, we analyzed the distribution of Bassoon and Piccolo at an earlier stage of ribbon development. [25] In the wt retina, although the pattern of coupling between Bassoon and Piccolo is less robust at P13 than at P16, synaptic ribbons are clearly visible (Fig. 2G; arrows indicate coupling). In comparison, in the P13 *tulp1*^{−/−} retina, the lack of coupling between Bassoon and Piccolo is already similar to that noted at P16, suggesting that normal ribbons may never form in the absence of Tulp1 (Fig. 2H).

We further examined synaptic terminal architecture using antibodies against Ribeye/CtBP2, a 120-kDa protein that constitutes the central scaffold of the ribbon and colocalizes with Piccolo and Bassoon.[2,29,37] Figure 3A shows that the P16 wt OPL contains a multitude of distinct horseshoe-shaped Ribeye-positive ribbons (arrows). Although the P16 *tulp1*^{−/−} retina contains few normal ribbons (Fig. 3B), a pattern similar to that of wt is seen in rd10 retinas at P16 (Fig. 3C) and P21 (Fig. 3D), before and after the commencement of retinal degeneration.

Given that ribbon-associated proteins exhibited structural abnormalities in the *tulp1*^{−/−} retinas at P13, we wondered whether defects might also be noted in the ribbon itself at this early stage of development. Although the P13 wt retina contains many distinct and well-formed ribbons (Fig. 3E), fewer ribbons are seen in the P13 *tulp1*^{−/−} retina (Fig. 3F). These results document distinct abnormalities in the young *tulp1*^{−/−} retina that are not shared with another model of early-onset photoreceptor degeneration.

## Mislocalized Rhodopsin Not Sufficient to Induce Synaptic Ribbon Abnormalities

Although rhodopsin is normally confined to the photoreceptor OS, it is distributed throughout *tulp1*^{−/−} photoreceptors.[18,20] It has been suggested that mislocalized rhodopsin causes photoreceptor degeneration, possibly because of an accumulation at the synapse.[38] This hypothesis suggests that protein mislocalization may interfere with synaptic ribbon architecture. To determine the association between rhodopsin mislocalization and photoreceptor synaptic structure, we examined rhodopsin distribution in rd10 and *tulp1*^{−/−} retinas at different ages. In the wt retina at P16, rhodopsin staining is confined to the OS (Fig. 4A). This is also the case in the rd10 retina at P16, before retinal degeneration (Fig. 4B). In comparison, rhodopsin is mislocalized to the IS, throughout the ONL, and within the photoreceptor terminals of the P21 rd10 retina (Fig. 4C), an age that corresponds to the highest rate of photoreceptor degeneration. [34,35] At this age, rhodopsin distribution is similar to that seen in the *tulp1*^{−/−} retina at P16 (Fig. 4D). Despite the evidence of rhodopsin mislocalization in the P21 rd10 retina, the normal configuration of Piccolo and Bassoon is preserved (Fig. 2D), and Ribeye-labeled ribbons are intact (Fig. 3D). These results indicate that displaced rhodopsin molecules are insufficient to alter photoreceptor synaptic ribbon architecture.

## Underdeveloped Bipolar Cell Dendrites in *tulp1*^{−/−} Mice

To investigate the consequences of the photoreceptor synaptic malformation on postsynaptic elements, we examined *tulp1*^{−/−} retinas using antibodies against PKC, which labels rod

DBCs and their respective dendrites.[39] At P16, wt DBC dendrites have elongated processes that penetrate the OPL, and each termination has a high degree of arborization (Fig. 5A). In comparison, DBC dendrites of P16 *tulp1*^{−/−} mice are shorter and display less branching or complexity (Fig. 5B). On the other hand, DBC terminals of the P16 rd10 retina resemble those of wt (Fig. 5C). DBC dendritic retraction was, however, noted in the P21 rd10 retina, which resembled the P16 *tulp1*^{−/−} phenotype (Fig. 5D).

To ascertain whether normal postsynaptic architecture might be noted earlier, we also examined P13 retinas using PKC staining. In the P13 wt retina, dendrite lengths were shorter and branching was sparser than in P16 retinas (Fig. 5E). In the P13 *tulp1*^{−/−} retina, however, DBC dendrites were difficult to differentiate from the DBC cell bodies, and branching was not observed (Fig. 5F). The presence of markedly reduced DBC dendrites early in the development of the *tulp1*^{−/−} retina suggested that normal dendrites were unlikely ever to form. In comparison, in the rd10 retina, it appeared that DBC dendrites first formed and then retracted in concert with the progressive photoreceptor degeneration, as previously noted.[35]

We quantified dendritic processes of DBCs identified by PKC labeling in wt, rd10, and *tulp1*^{−/−} mice at P16 at central and peripheral locations (Fig. 6). For each genotype, we examined four different PKC-immunoreactive retinas. Dendrite lengths were measured over the entire area of the image, averaged per genotype, and reported as deriving from the central retina (within 200 µm of the optic nerve) or peripheral retina (within 200 µm of the periphery). Figure 6A presents a low-power image of the inferior wt retina; PKC immunofluorescence is shown as white, and boxes indicate the central and peripheral locations examined. Figure 6 also shows representative higher power images of corresponding central (Figs. 6B, C) and peripheral (Figs. 6D, E) areas of wt and *tulp1*^{−/−} retinas. In each panel, the yellow vertical lines indicate the dendrite lengths. Average dendritic lengths (± SEM) are summarized in Figures 6F and 6G for central and peripheral locations, respectively. In the central retina, no significant differences in dendritic length were seen between wt and rd10 (12.93 µm ± 1.1 vs. 12.58 µm ± 0.8; $P = 0.786$). In the same region; however, average dendrite length was statistically significantly shorter in *tulp1*^{−/−} than in wt (7.29 µm ± 0.8 vs. 12.93 µm ± 1.1; $P = 0.006$) retinas. Similar results were seen in the peripheral retina (Fig. 6G), in which average dendrite length was shorter in *tulp1*^{−/−} than in wt (5.46 µm ± 0.58 vs. 8.09 µm ± 0.2; $P = 0.005$) retinas, whereas no difference was detected between rd10 and wt (8.26 µm ± 0.68 vs. 8.09 µm ± 0.2; $P = 0.820$) retinas. Thus, DBC dendrites were markedly abnormal at central and peripheral regions in P16 *tulp1*^{−/−} retinas, with an average reduction in DBC dendritic length of 33% to 44%. We observed shorter DBC dendrites in the peripheral retina, which we believe was related to the gradient of neurogenesis from the center to the periphery of the retina.[40] These data indicate that the structural platform for relaying signaling from photoreceptors to the inner retina is underdeveloped or malformed in *tulp1*^{−/−} mice.

To define the relationship between the presynaptic and postsynaptic photoreceptor elements, P16 retinas were labeled for PKC and Bassoon. In wt mice (Fig. 7A), PKC-positive DBC dendrites (left panel) and Bassoon-positive ribbons (middle panel) appeared to interact closely (right panel). In comparison, *tulp1*^{−/−} DBC dendrites and Bassoon-labeled ribbons displayed structural defects (Fig. 7B). In the *tulp1*^{−/−} retina, DBC dendrites and presynaptic ribbons were, nevertheless, closely apposed and confined to the OPL, providing at least a minimal platform for photoreceptor-to-bipolar cell transmission.

## Reduced and Less Sensitive ERG b-Wave in *tulp1*^{−/−} Mice

We used dark-adapted ERG recordings to evaluate outer retinal function in the P16 mice studied here. From these recordings, we extracted parameters related to photoreceptor function (equation 2) and DBC activity (equation 1). Figure 8 presents representative

responses obtained from wt, *tulp1*$^{+/-}$, *tulp1*$^{-/-}$, and rd10 mice to strobe flash stimuli presented after overnight dark adaptation (Fig. 8A) and summary intensity-response functions for the ERG a-wave (Fig. 8B) and b-wave (Fig. 8C). At P16, wt responses have distinct a- and b-waves, as expected from earlier reports, and indicate the presence of functional invaginating synapses between rod photoreceptors and rod DBCs.[41] Responses of *tulp1*$^{+/-}$ mice were comparable to those of wt animals, as previously reported.[18] In comparison to wt and *tulp1*$^{+/-}$ data, responses of *tulp1*$^{-/-}$ and rd10 mice were reduced in amplitude and had delayed b-wave implicit times.

We used equations 1 and 2 to examine the b-wave intensity-response function and the leading edge of the a-wave, respectively. There was no difference in any parameter between wt and *tulp1*$^{+/-}$ data. In comparison, the amplitude parameters $R_{max}$ and *RmP3* were significantly ($P < 0.002$) reduced in *tulp1*$^{-/-}$ and rd10 mice. However, effects on the sensitivity parameters $K$ and $A$ were strain specific. Compared with wt or *tulp1*$^{+/-}$ data, values of $K$ were significantly elevated in *tulp1*$^{-/-}$ mice but not in rd10 animals. This analysis confirms the impression from Figure 8C that the rd10 b-wave intensity-response function is shifted only downward from the wt or *tulp1*$^{+/-}$ functions, whereas the *tulp1*$^{+/-}$ function appears to be shifted down and to the right along the stimulus-intensity axis.

Figure 8D plots the leading edge of the a-waves obtained to a high-intensity stimulus for each genotype studied. Each trace represents the average of all mice tested, after which the a-wave trough was normalized to $-1.0$.[42] In this representation, it is clear that there is substantial overlap between the responses of wt, *tulp1*$^{+/-}$, and *tulp1*$^{-/-}$ mice, whereas the rd10 response is substantially slower. Given this, it is not surprising that when equation 2 was fit to individual data, the values of $A$ obtained for *tulp1*$^{-/-}$ mice were not different from those of wt or *tulp1*$^{+/-}$ mice but were significantly ($P < 0.001$) decreased in rd10 mice.

By obtaining parameters that correspond to OS phototransduction gain ($A$) and DBC sensitivity ($K$), we can begin to examine signal transmission through the retina. Figure 8E plots values of $A$ and $K$ for wt mice and the three mutant genotypes studied here (*tulp1*$^{-/-}$, *tulp1*$^{+/-}$, and rd10), all compared with the wt average. In this format, reduced phototransduction gain, corresponding to lower values of $A$, fall below the wt point, whereas reduced DBC sensitivity, corresponding to higher values of $K$, fall to the right of the wt point. The *tulp1*$^{+/-}$ data fall near wt in both dimensions, consistent with normal photoreceptor and DBC function in heterozygotes. For *tulp1*$^{-/-}$ mice, the main departure from wt is a rightward shift along the $K$ axis, indicating that more light is required to generate a b-wave. In comparison, the main departure from wt for rd10 mice is a downward shift to lower values of $A$, indicating a reduction in phototransduction gain.

## DISCUSSION

It is well established that mutations in *TULP1* underlie a severe form of photoreceptor degeneration.[7–10] Herein, we present evidence that Tulp1 is required for the formation of normal synapses at the photoreceptor terminal. The association of early-onset and severe photoreceptor degeneration with rhodopsin mislocalization, which is preceded by synaptic abnormalities, appears to represent a phenotype that has not been described previously.

### Malformation of *tulp1*$^{-/-}$ Photoreceptor Synapses

In young *tulp1*$^{-/-}$ mice, two key ribbon-associated proteins, Piccolo and Bassoon, are rarely united into the horseshoe shape characteristic of the wt photoreceptor ribbon synaptic complex. The proteins are, however, situated close to one another and are confined to the OPL. These observations indicate that in the absence of Tulp1, Piccolo and Bassoon are able to arrive at their correct destinations but are unable to coordinate into the normal synaptic

architecture. In addition, immunostaining for Ribeye showed that few intact ribbons were present in the *tulp1*$^{-/-}$ retina.

Before or during the height of photoreceptor degeneration, normal synaptic architecture is readily seen in the rd10 retina. This does not necessarily indicate that the observed synaptic defects are unique to the *tulp1*$^{-/-}$ retina, but it does make clear that generalized photoreceptor degeneration is not sufficient to induce synaptic alterations. Moreover, it appears that these abnormalities in ribbon-associated proteins are specific to mutations involving proteins that are critical for photoreceptor synapse formation. In general, these mice exhibit abnormalities in ribbon-associated proteins and dramatically diminished b-waves concomitant with altered DBC composition. An example of a mutation primarily affecting the synapse comes from a line of mice lacking Bassoon. In Bassoon-deficient mice (*Bsn*$^{-/-}$), Ribeye and Piccolo staining is also punctate, but contrary to what occurs in the *tulp1*$^{-/-}$ retina, they still colocalize (GHG, unpublished data, 2008).[29] The loss of Bassoon results in free-floating ribbons, splitting the presynaptic apparatus into the "ribbon-associated complex," including Ribeye and Piccolo, and the "plasma membrane/arciform density-associated complex."[29] In *tulp1*$^{-/-}$ mice, the proteins affiliated with the ribbon-associated complex are in disarray; in *Bsn*$^{-/-}$ mice, the ribbon-associated complex is thought to be intact but not anchored to the presynaptic membrane. In both cases, we hypothesize that the capacity to signal second-order neurons would be greatly diminished. In addition to exhibiting attenuated dendrites similar to those in *tulp1*$^{-/-}$ mice, *Bsn*$^{-/-}$ mice develop ectopic photoreceptor terminals and sprouting dendritic projections in the ONL, a feature that makes them closely resemble two other presynaptic mouse mutants, *Cabp4*$^{-/-}$ and *Cacna1f*$^{nob2}$.[27,28] Although it is not fully known why ectopic photoreceptor synapses form in these mutants, they all share an alteration in calcium channel function.[28] To date, there is no link between Tulp1 and calcium movement. Moreover, the *tulp1*$^{-/-}$ phenotype does not involve ectopic sprouting, suggesting that the absence of Tulp1 may alter synaptic structure by a distinct mechanism. It is important to note that appreciable photoreceptor degeneration is not observed in *Cabp4*$^{-/-}$, *Bsn*$^{-/-}$, or *Cacna1f*$^{nob2}$ mice.[27–29] Taken together, these data indicate that the synaptic abnormalities and severe photoreceptor degeneration noted in *tulp1*$^{-/-}$ mice reflect distinct defects and indicate that Tulp1 plays multiple roles in photoreceptor cells.

## Mislocalized Rhodopsin Not Sufficient to Disrupt Synaptic Architecture in *tulp1*$^{-/-}$ Mice

Rhodopsin mislocalization has been observed in numerous animal models of retinal degeneration. Regardless of the underlying cause, it is believed that the buildup of mislocalized rhodopsin throughout the photoreceptor induces pathologic changes that ultimately lead to cell death.[38] It has been proposed that the primary pathologic change in photoreceptors is the alteration of structural and functional aspects of membranes because of the constant delivery and lack of removal of ectopic rhodopsin.[38] It has been further postulated that the synapse would be particularly susceptible to "membrane crowding" by rhodopsin molecules, which would interfere with the highly regulated and dynamic processes of exocytosis and endocytosis.[38] This hypothesis raises the possibility that mislocalized rhodopsin in the *tulp1*$^{-/-}$ mice might disrupt the normal ribbon architecture, which is closely linked to the presynaptic membrane. In the rd10 retina, we noted that rhodopsin mislocalization occurs after the onset of degeneration, which is in agreement with the findings of a recent study.[43] However, before and during retinal degeneration, the normal coupling between Piccolo and Bassoon is retained and the ribbons are intact. This finding indicates that mislocalized rhodopsin molecules are not sufficient to disrupt normal photoreceptor synaptic ribbon architecture and implicates the absence of Tulp1 in the synapse as the primary cause of ribbon malformation in *tulp1*$^{-/-}$ mice.

## Underdeveloped Bipolar Cell Dendrites in *tulp1*^{−/−} Mice

In many mutant mouse models, reduced inner retinal processes have been shown to occur secondarily to photoreceptor degeneration or anomalous development.[35,44,45] Here we show that mice lacking Tulp1 have a reduced dendritic composition that precedes photoreceptor degeneration. Because photoreceptor presynaptic structural defects occur in the *tulp1*^{−/−} retina, we hypothesize that there should be a reduction in the signal output potential. The attenuation of photoreceptor signaling has been previously linked to subsequent alterations in the adjacent neural layers of the retina.[45,46] In *tulp1*^{−/−} mice, there is a profound shortening of individual dendrites and a severe attenuation of dendrite branching in the central and the peripheral retina. The atrophy of postsynaptic dendritic processes has been observed in many models of retinal degeneration and has been termed *retraction* to denote the negative remodeling from an earlier developed state as a direct and downstream effect of photoreceptor cell death, regardless of the underlying genetic cause of retinal degeneration. [35,45] This retraction response is thought to be initiated by a lack of signaling or trophic factors, no longer able to be delivered because of absent photoreceptor terminals.[35,45,46] However, in the *tulp1*^{−/−} retina, shortened dendrite lengths and reduced branching are detected *before* photoreceptor cell death. Therefore, we conclude that the reduction of the DBC dendritic field in the *tulp1*^{−/−} retina is a developmental consequence of an attenuated trophic and transmitter release that would be expected from a presynaptic malformation. This is in contrast to the rd10 retina, in which reduction in length and branching of bipolar dendrites are observed only *after* the commencement of photoreceptor cell death (P21). It is important to note that *tulp1*^{−/−} DBC dendrites lengthen between P13 to P16. However, this developmental process never achieves a normal configuration. Given the abnormalities in rd10 mice at P21, we predict a further reduction from the modest DBC dendrites noted in *tulp1*^{−/−} mice at later ages concomitant with maximal photoreceptor degeneration.

## Two Distinct Functional Abnormalities in *tulp1*^{−/−} Mice

ERG study results of young *tulp1*^{−/−} mice indicate the presence of two functional defects. One defect occurs at the level of the photoreceptor OS, which generates the dark-adapted a-wave.[47] Although photoreceptor loss is not evident at P16, the *tulp1*^{−/−} a-wave is already reduced in amplitude. Despite the overall reduction of the *tulp1*^{−/−} ERG a-wave, the leading edge of the a-wave had normal gain. This is readily seen when responses are normalized for overall amplitude. A similar conclusion applies to ERG a-waves obtained from P15 *tulp1*^{−/−} mice.[22] Although a comparable a-wave reduction is noted in P16 rd10 mice, this reduction appears to reflect the initial stages of rod degeneration and a lower phototransduction gain. This latter result was confirmed by applying the same analysis to ERG a-waves obtained in another study from rd10 mice at P18 and P30.[34]

A second defect noted in *tulp1*^{−/−} mice occurs at the level of b-wave generation, which, under these stimulus conditions, reflects the activity of rod DBCs subsequent to rod photoreceptor input.[47] Reduced b-wave amplitude was expected in the presence of an a-wave reduction, and this result was noted in *tulp1*^{−/−} and rd10 mice. However, our analysis showed that the b-wave intensity-response function was also shifted to the right along the intensity axis for P16 *tulp1*^{−/−} mice but not for age-matched rd10 animals. Although fewer intensity settings were used, earlier ERG results obtained from P15 *tulp1*^{−/−} mice[22] show changes similar to those noted here for P16 *tulp1*^{−/−} animals. We speculate that the overall amplitude reduction is associated with a decreased photoreceptor response and that the rightward shift, seen only in *tulp1*^{−/−} mice, reflects the abnormalities in ribbon synapse architecture and DBC dendrite structure documented anatomically in these animals.

In conclusion, the absence of Tulp1 results in abnormalities that affect structure and function in multiple retinal sites. The photoreceptor degeneration and OS defects of *tulp1*^{−/−} mice

have been described, providing evidence that Tulp1 may function in the polarized transport of proteins at the apical end of the photoreceptor.[18,20] We have shown that Tulp1 interacts with Actin and Dynamin-1, two proteins known to be critical in the cytoskeletal scaffold and involved in the molecular pathway of vesicular protein transport occurring from the inner segment to the outer segment and in vesicle cycling at terminals of photoreceptors.[2,3] Interestingly, in *tulp1*$^{-/-}$ mice, Dynamin-1 staining in the synapse is greatly attenuated (GHG, unpublished data, 2008), raising the possibility that Tulp1 and Dynamin-1 are in the same pathway. Thus, Tulp1 may function in intracellular protein trafficking throughout the photoreceptor cell, and, in its absence, two distinct abnormalities at polar ends of the cell are highlighted. Here we provide evidence that photoreceptor ribbon synapses and DBC dendrites are also severely affected at an early age. These new findings indicate that Tulp1 is essential for photoreceptor cell survival and is required for the proper development of the photoreceptor synapse. It will be interesting to learn whether similar synaptic defects are present in human patients carrying *TULP1* mutations.

## Acknowledgments

## References

1. tom Dieck S, Brandstätter JH. Ribbon synapses of the retina. Cell Tissue Res 2006;326(2):339–346. [PubMed: 16775698]

2. Schmitz F, Königstorfer A, Südhof TC. RIBEYE, a component of synaptic ribbons: a protein's journey through evolution provides insight into synaptic ribbon function. Neuron 2000;28(3):857–872. [PubMed: 11163272]

3. Morgans CW. Presynaptic proteins of ribbon synapses in the retina. Microsc Res Tech 2000;50(2):141–150. [PubMed: 10891878]

4. Chang B, Heckenlively JR, Bayley PR, et al. The nob2 mouse, a null mutation in Cacna1f: anatomical and functional abnormalities in the outer retina and their consequences on ganglion cell visual responses. Vis Neurosci 2006;23(1):11–24. [PubMed: 16597347]

5. Boughman JA, Conneally PM, Nance WE. Population genetic studies of retinitis pigmentosa. Am J Hum Genet 1980;32(2):223–235. [PubMed: 7386458]

6. Bunker CH, Berson EL, Bromley WC, Hayes RP, Roderick TH. Prevalence of retinitis pigmentosa in Maine. Am J Ophthalmol 1984;97(3):357–365. [PubMed: 6702974]

7. Hagstrom SA, North MA, Nishina PM, Berson EL, Dryja TP. Recessive mutations in the gene encoding the tubby-like protein TULP1 in patients with retinitis pigmentosa. Nat Genet 1998;18(2):174–176. [PubMed: 9462750]

8. Banerjee P, Kleyn PW, Knowles JA, et al. TULP1 mutation in two extended Dominican kindreds with autosomal recessive retinitis pigmentosa. Nat Genet 1998;18(2):177–179. [PubMed: 9462751]

9. Gu S, Lennon A, Li Y, et al. Tubby-like protein-1 mutations in autosomal recessive retinitis pigmentosa. Lancet 1998;351(9109):1103–1104. [PubMed: 9660588]

10. Paloma E, Hjelmqvist L, Bayés M, et al. Novel mutations in the TULP1 gene causing autosomal recessive retinitis pigmentosa. Invest Ophthalmol Vis Sci 2000;41(3):656–659. [PubMed: 10711677]

11. North MA, Naggert JK, Yan Y, Noben-Trauth K, Nishina PM. Molecular characterization of TUB, TULP1, and TULP2, members of the novel tubby gene family and their possible relation to ocular diseases. Proc Natl Acad Sci U S A 1997;94(7):3128–3133. [PubMed: 9096357]

12. Kleyn PW, Fan W, Kovats SG, et al. Identification and characterization of the mouse obesity gene tubby: a member of a novel gene family. Cell 1996;85(2):281–290. [PubMed: 8612280]

13. Nishina PM, North MA, Ikeda A, Yan Y, Naggert JK. Molecular characterization of a novel tubby gene family member, TULP3, in mouse and humans. Genomics 1998;54(2):215–220. [PubMed: 9828123]

14. Sahly I, Gogat K, Kobetz A, et al. Prominent neuronal-specific tub gene expression in cellular targets of tubby mice mutation. Hum Mol Genet 1998;7(9):1437–1447. [PubMed: 9700199]

15. Ikeda S, He W, Ikeda A, Naggert JK, North MA, Nishina PM. Cell-specific expression of tubby gene family members (tub, Tulp1, 2, and 3) in the retina. Invest Ophthalmol Vis Sci 1999;40(11): 2706–2712. [PubMed: 10509669]

16. He W, Ikeda S, Bronson RT, et al. GFP-tagged expression and immunohistochemical studies to determine the subcellular localization of the tubby gene family members. Brain Res Mol Brain Res 2000;81(1–2):109–117. [PubMed: 11000483]

17. Ohlemiller KK, Hughes RM, Mosinger-Ogilvie J, Speck JD, Grosof DH, Silverman MS. Cochlear and retinal degeneration in the tubby mouse. Neuroreport 1995;6(6):845–849. [PubMed: 7612867]

18. Hagstrom SA, Duyao M, North MA, Li T. Retinal degeneration in tulp1$^{-/-}$ mice: vesicular accumulation in the interphotoreceptor matrix. Invest Ophthalmol Vis Sci 1999;40(12):2795– 2802. [PubMed: 10549638]

19. Ikeda S, Shiva N, Ikeda A, et al. Retinal degeneration but not obesity is observed in null mutants of the tubby-like protein 1 gene. Hum Mol Genet 2000;9(2):155–163. [PubMed: 10607826]

20. Hagstrom SA, Adamian M, Scimeca M, Pawlyk BS, Yue G, Li T. A role for the Tubby-like protein 1 in rhodopsin transport. Invest Ophthalmol Vis Sci 2001;42(9):1955–1962. [PubMed: 11481257]

21. Xi Q, Pauer GJ, Marmorstein AD, Crabb JW, Hagstrom SA. Tubby-like protein 1 (TULP1) interacts with F-actin in photoreceptor cells. Invest Ophthalmol Vis Sci 2005;46(12):4754–4761. [PubMed: 16303976]

22. Xi Q, Pauer GJ, Ball SL, et al. Interaction between the photoreceptor-specific tubby-like protein 1 and the neuronal-specific GTPase dynamin-1. Invest Ophthalmol Vis Sci 2007;48(6):2837–2844. [PubMed: 17525220]

23. van der Bliek AM. Functional diversity in the dynamin family. Trends Cell Biol 1999;9(3):96–102. [PubMed: 10201074]

24. McNiven MA, Cao H, Pitts KR, Yoon Y. The dynamin family of mechanoenzymes: pinching in new places. Trends Biochem Sci 2000;25(3):115–120. [PubMed: 10694881]

25. Dick O, tom Dieck S, Altrock WD, et al. The presynaptic active zone protein bassoon is essential for photoreceptor ribbon synapse formation in the retina. Neuron 2003;37(5):775–786. [PubMed: 12628168]

26. Chang B, Hawes NL, Hurd RE, Davisson MT, Nusinowitz S, Heckenlively JR. Retinal degeneration mutants in the mouse. Vision Res 2002;42(4):517–525. [PubMed: 11853768]

27. Haeseleer F, Imanishi Y, Maeda T, et al. Essential role of Ca$^{2+}$-binding protein 4, a Cav1.4 channel regulator, in photoreceptor synaptic function. Nat Neurosci 2004;7(10):1079–1087. [PubMed: 15452577]

28. Bayley PR, Morgans CW. Rod bipolar cells and horizontal cells form displaced synaptic contacts with rods in the outer nuclear layer of the nob2 retina. J Comp Neurol 2007;500(2):286–298. [PubMed: 17111373]

29. tom Dieck S, Altrock WD, Kessels MM, et al. Molecular dissection of the photoreceptor ribbon synapse: physical interaction of Bassoon and RIBEYE is essential for the assembly of the ribbon complex. J Cell Biol 2005;168(5):825–836. [PubMed: 15728193]

30. Peachey NS, Alexander KR, Fishman GA. The luminance-response function of the dark-adapted human electroretinogram. Vision Res 1989;29(3):263–270. [PubMed: 2788958]

31. Lamb TD, Pugh EN Jr. A quantitative account of the activation steps involved in phototransduction in amphibian photoreceptors. J Physiol 1992;449:719–758. [PubMed: 1326052]

32. Pugh EN Jr, Lamb TD. Amplification and kinetics of the activation steps in phototransduction. Biochim Biophys Acta 1993;1141(2–3):111–149. [PubMed: 8382952]

33. Dick O, Hack I, Altrock WD, Garner CC, Gundelfinger ED, Brandstätter JH. Localization of the presynaptic cytomatrix protein Piccolo at ribbon and conventional synapses in the rat retina: comparison with Bassoon. J Comp Neurol 2001;439(2):224–234. [PubMed: 11596050]

34. Chang B, Hawes NL, Pardue MT, et al. Two mouse retinal degenerations caused by missense mutations in the beta-subunit of rod cGMP phosphodiesterase gene. Vision Res 2007;47(5):624–633. [PubMed: 17267005]

35. Gargini C, Terzibasi E, Mazzoni F, Strettoi E. Retinal organization in the retinal degeneration 10 (rd10) mutant mouse: a morphological and ERG study. J Comp Neurol 2007;500(2):222–238. [PubMed: 17111372]

36. Landmann L, Marbet P. Colocalization analysis yields superior results after image restoration. Microsc Res Tech 2004;64(2):103–112. [PubMed: 15352081]

37. Heidelberger R, Thoreson WB, Witkovsky P. Synaptic transmission at retinal ribbon synapses. Prog Retin Eye Res 2005;24(6):682–720. [PubMed: 16027025]

38. Deretic D. A role for rhodopsin in a signal transduction cascade that regulates membrane trafficking and photoreceptor polarity. Vision Res 2006;46(27):4427–4433. [PubMed: 17010408]

39. Greferath U, Grünert U, Wässle H. Rod bipolar cells in the mammalian retina show protein kinase C-like immunoreactivity. J Comp Neurol 1990;301(3):433–442. [PubMed: 2262600]

40. Finlay BL. The developing and evolving retina: using time to organize form. Brain Res 2008;1192:5–16. [PubMed: 17692298]

41. Keeler CE, Sutcliffe E, Chaffee EL. A description of the ontogenetic development of retinal action currents in the house mouse. Proc Natl Acad Sci U S A 1928;14(10):811–815. [PubMed: 16587413]

42. Ren JC, LaVail MM, Peachey NS. Retinal degeneration in the nervous mutant mouse, III: electrophysiological studies of the visual pathway. Exp Eye Res 2000;70(4):467–473. [PubMed: 10865995]

43. Barhoum R, Martínez-Navarrete G, Corrochano S, et al. Functional and structural modifications during retinal degeneration in the rd10 mouse. Neuroscience 2008;155(3):698–713. [PubMed: 18639614]

44. Pignatelli V, Cepko CL, Strettoi E. Inner retinal abnormalities in a mouse model of Leber's congenital amaurosis. J Comp Neurol 2004;469(3):351–359. [PubMed: 14730587]

45. Marc RE, Jones BW, Watt CB, Strettoi E. Neural remodeling in retinal degeneration. Prog Retin Eye Res 2003;22(5):607–655. [PubMed: 12892644]

46. Léveillard T, Mohand-Saïd S, Lorentz O, et al. Identification and characterization of rod-derived cone viability factor. Nat Genet 2004;36(7):755–759. [PubMed: 15220920]

47. Frishman, LJ. Origins of the electroretinogram. In: Heckenlively, JR.; Arden, GB., editors. Principles and Practice of Clinical Electrophysiology of Vision. 2nd ed.. Cambridge, MA: MIT Press; 2006. p. 139-183.
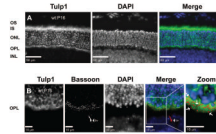
**FIGURE 1.**
Tulp1 is localized to the photoreceptor synapse. (**A**) Immunofluorescent localization of Tulp1 (*green*) and nuclei (DAPI; *blue*) in wt mouse retinal sections. (**B**) Higher power image of the OPL of the wt retina. Tulp1 (*green*), synaptic protein Bassoon (*red*), and nuclei (*blue*). The final panel is a digital magnification; *arrows* indicate that Tulp1 and Bassoon colocalize to the photoreceptor synaptic terminals. bv, blood vessel.
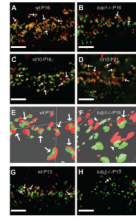
**FIGURE 2.**

Photoreceptor synaptic ribbon-associated proteins are abnormal in the *tulp1*$^{-/-}$ retina. Deconvolution-generated images of immunofluorescent localization of Bassoon (*green*) and Piccolo (*red*) in the OPL of mouse retinal sections. In the wt OPL at P16 (**A**), rd10 at P16 (**C**), and P21 (**D**), the horseshoe-like appearances of the photoreceptor synaptic ribbons are clearly visible. *Arrows* highlight the tight coupling between Bassoon and Piccolo, composing individual ribbons. In the *tulp1*$^{-/-}$ OPL at P16 (**B**), the ribbons appear to exhibit morphologic abnormalities, possibly indicating a structural ribbon defect. To best show the distinction between the proximity and coupling of Bassoon and Piccolo at P16, three-dimensional surface plots were generated from a portion of the 2-µm Z-stacks of wt (**A**) and *tulp1*$^{-/-}$ (**B**) retinas. In the wt retina (**E**), *arrows* point to the union of Bassoon and Piccolo, forming the compact horseshoe-shaped ribbons. In the *tulp1*$^{-/-}$ retina (**F**), both proteins are present and in immediate proximity; however, they are not spatially fixed, as they are in the wt retina, into the normal horseshoe-shaped ribbon formation (*arrow* points to the union of Bassoon and Piccolo; *arrowheads* point to the separate ribbon staining of Bassoon and Piccolo). Early in the development of the wt functional synapse (P13), the coupling of the two proteins is not as robust (**G**) compared with the more mature P16 wt OPL (**A**); however, individual synaptic ribbons can be observed (*arrows* show coupling). In the *tulp1*$^{-/-}$ OPL at P13 (**H**), the ribbons exhibit the same abnormalities as P16, possibly indicating that the deficits of the ribbon are present throughout development. Scale bar, 5 µm; gridlines, 10 µm.
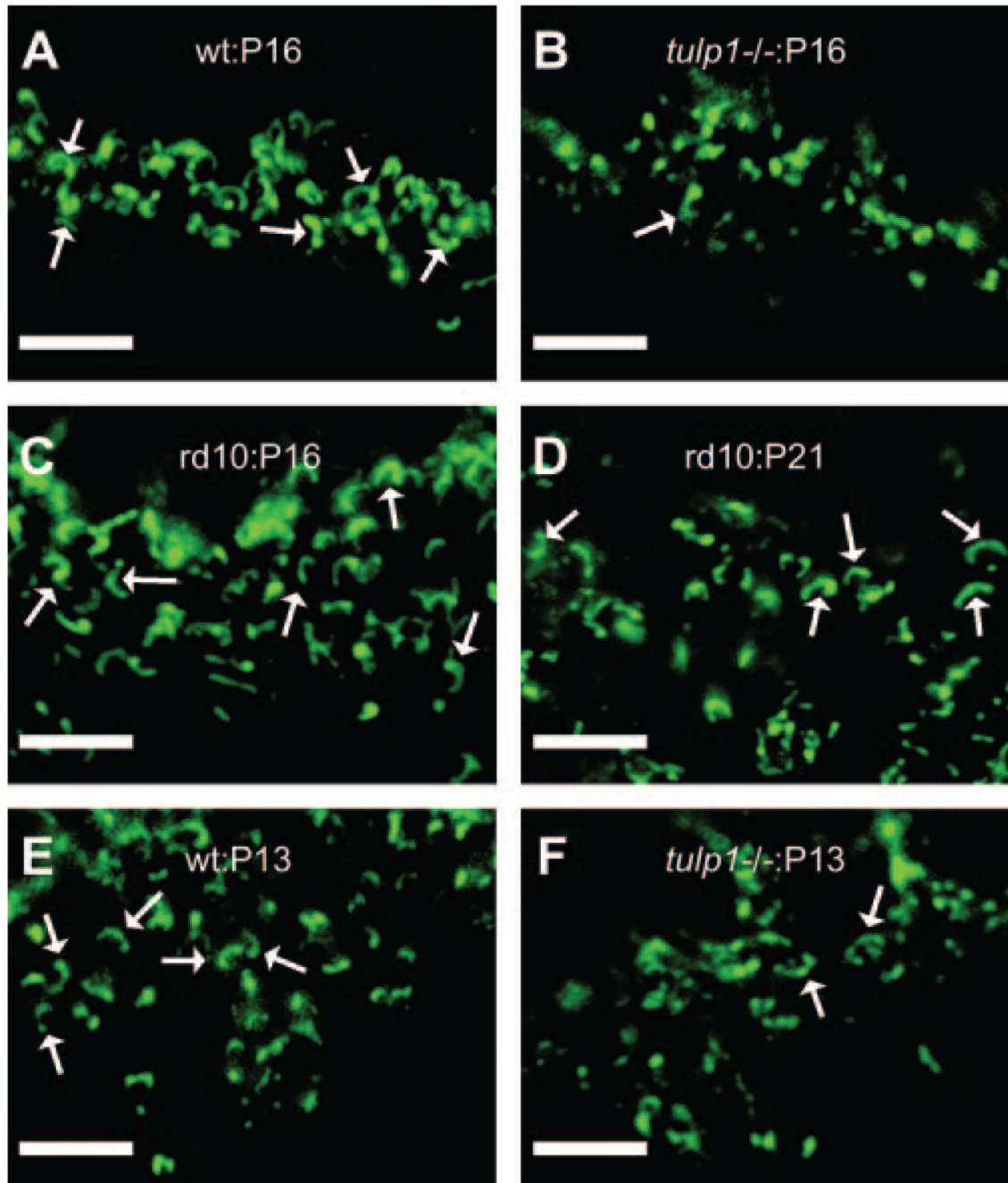
**FIGURE 3.**
The central ribbon protein, ribeye, is abnormal in the *tulp1*⁻/⁻ retina. Deconvolution-generated images of immunofluorescent localization of Ribeye/CtBP2 (*green*) in the OPL of mouse retinal sections. In the wt OPL at P16 (**A**), rd10 at P16 (**C**), and P21 (**D**), the horseshoe-like appearance of the synaptic ribbons is distinct (*arrows*). This is also the case in the wt OPL early in development (**E**). In the *tulp1*⁻/⁻ OPL at P13 (**F**) and P16 (**B**), the ribbons appear to exhibit morphologic abnormalities. The ribbons change from the classic horseshoe shape to diffuse immunoreactive areas, further raising the possibility of a synaptic malformation in the *tulp1*⁻/⁻ retina. Scale bar, 5 μm.
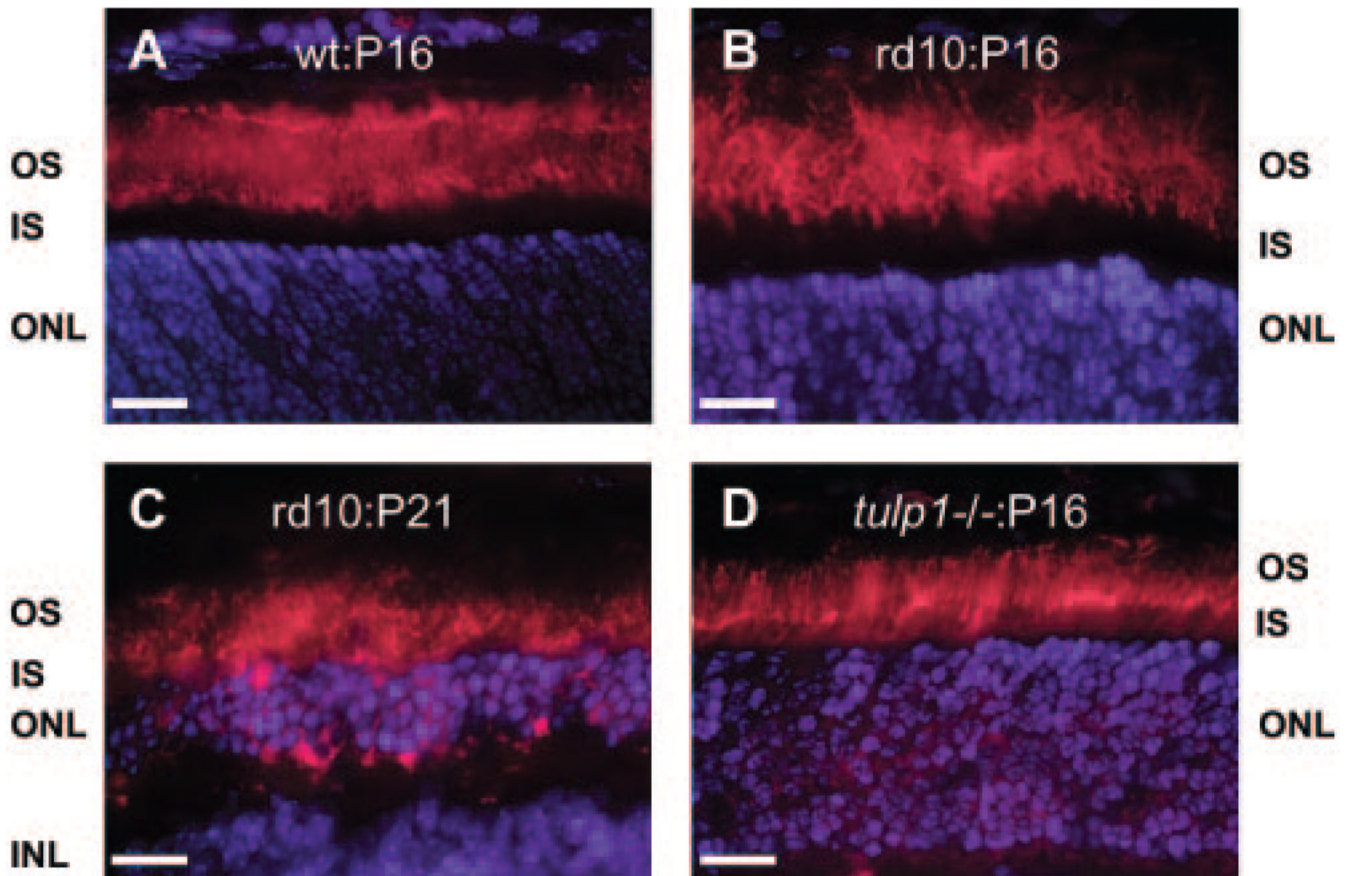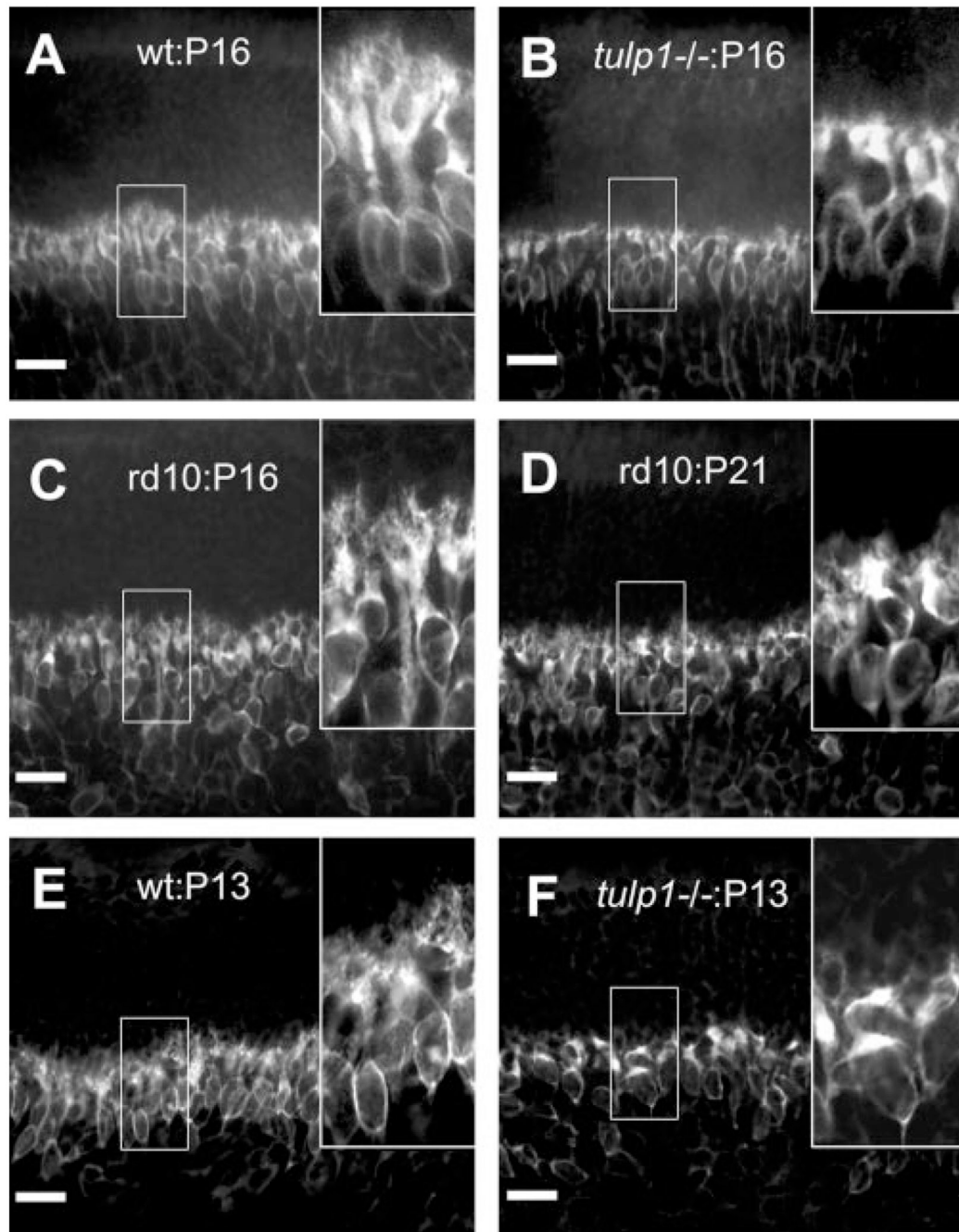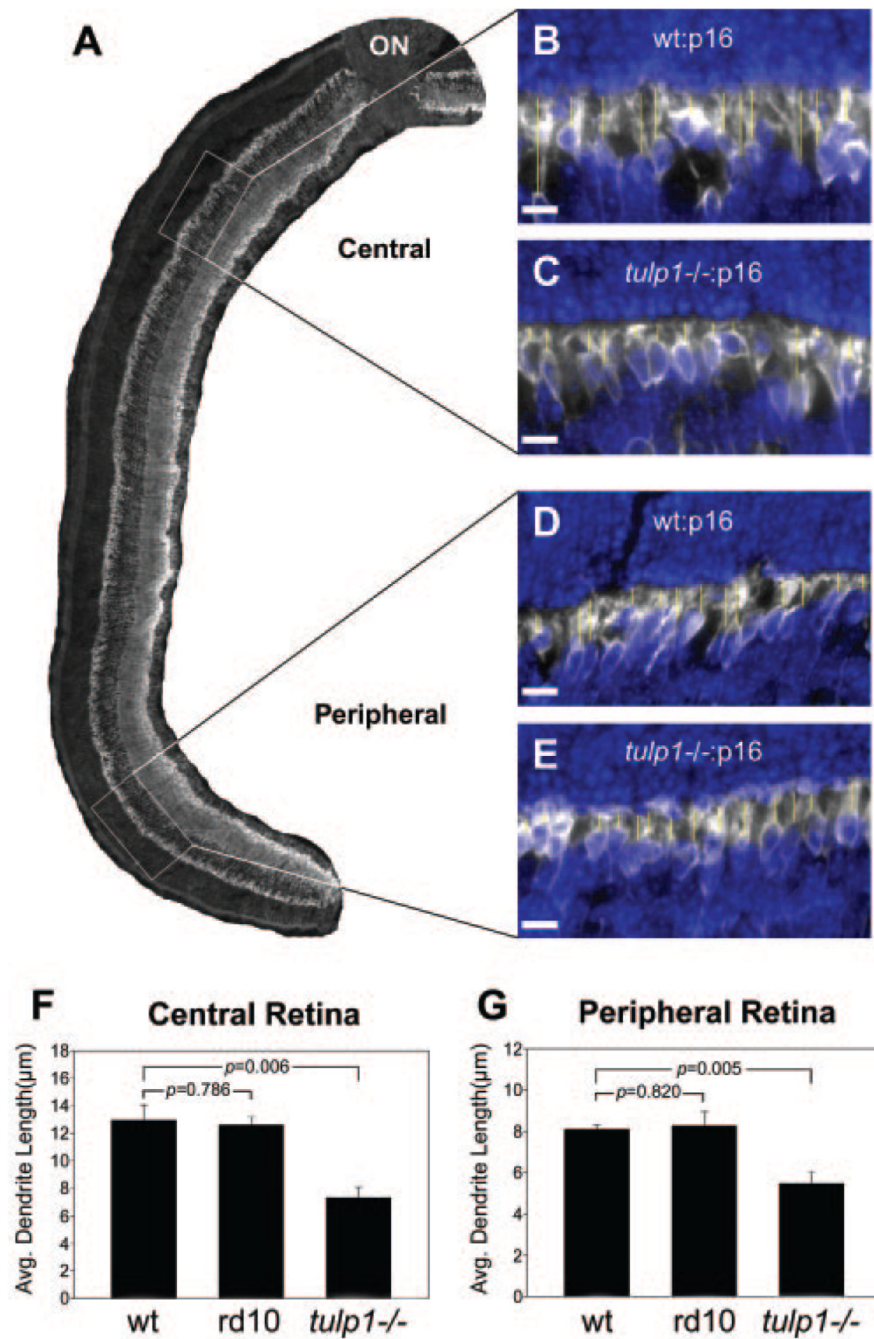
**FIGURE 4.**
Rhodopsin is mislocalized in *tulp1*^{−/−} and rd10 retinas. Immunofluorescent localization of rhodopsin (*red*) in mouse retinal sections (DAPI; *blue*). In the wt retina at P16 (**A**), rhodopsin staining in restricted to the OS. Rhodopsin is also confined to the OS in the rd10 retina at P16 (**B**), although the OS shows some signs of disorganization. In contrast, during the period of maximal degeneration at P21 (**C**), rhodopsin is severely mislocalized, with staining appearing in the IS, throughout the ONL, and within the photoreceptor terminals of the rd10 retina. As previously reported,[20] rhodopsin is mislocalized in *tulp1*^{−/−} retina at P16 (**D**). Scale bars, 20 µm.

**FIGURE 5.**
Bipolar cell dendrites are abnormal in the *tulp1*−/− retina. PKC immunofluorescent staining
of rod bipolar cell bodies in the INL with processes extending into the OPL. *Insets*: high
magnification, illustrating representative lengths and branching of the bipolar dendrites. In
wt at P16 (**A**), the dendritic field is robust, with long processes penetrating the OPL and
terminating with a high degree of arborization. This is in contrast to *tulp1*−/− at P16 (**B**),
where the dendrites appear as short appendages and branching has been severely attenuated.
rd10 retinas at P16 (**C**) and P21 (**D**) show some signs of disorganization of the bipolar
layers; however, it is only at P21 that retraction of the dendrites results in lengths
comparable to those of *tulp1*−/− at P16. In wt OPL at the early time point of P13 (**E**),

dendrite lengths are shorter and branching is abbreviated compared with the wt at P16. However, in the *tulp1*$^{-/-}$ OPL at P13 (**F**), dendrites are difficult to differentiate from the bipolar cell bodies and branching is not observed, possibly indicating that the dendrites are poorly developed and never mature properly. Scale bars, 10 µm.

**FIGURE 6.**
Bipolar cell dendritic field is attenuated in the *tulp1*$^{-/-}$ retina. (**A**) A montage of photomicrographs of the inferior mouse retina, immunostained for PKC. *White boxes* indicate the regions analyzed to quantify the dendritic field in P16 mice. Representative images of wt (**B**, **D**) and *tulp1*$^{-/-}$ (**C**, **E**) retinas analyzed from the central and peripheral regions, respectively. *Yellow lines* indicate the measurements of individual dendrites. The average dendrite length was statistically significantly shorter in both the central (**F**; *P* = 0.006) and the peripheral (**G**; *P* = 0.005) regions in *tulp1*$^{-/-}$ retinas compared with the wt. Data bars are the average ± SEM for four mice. Scale bars, 10 μm.
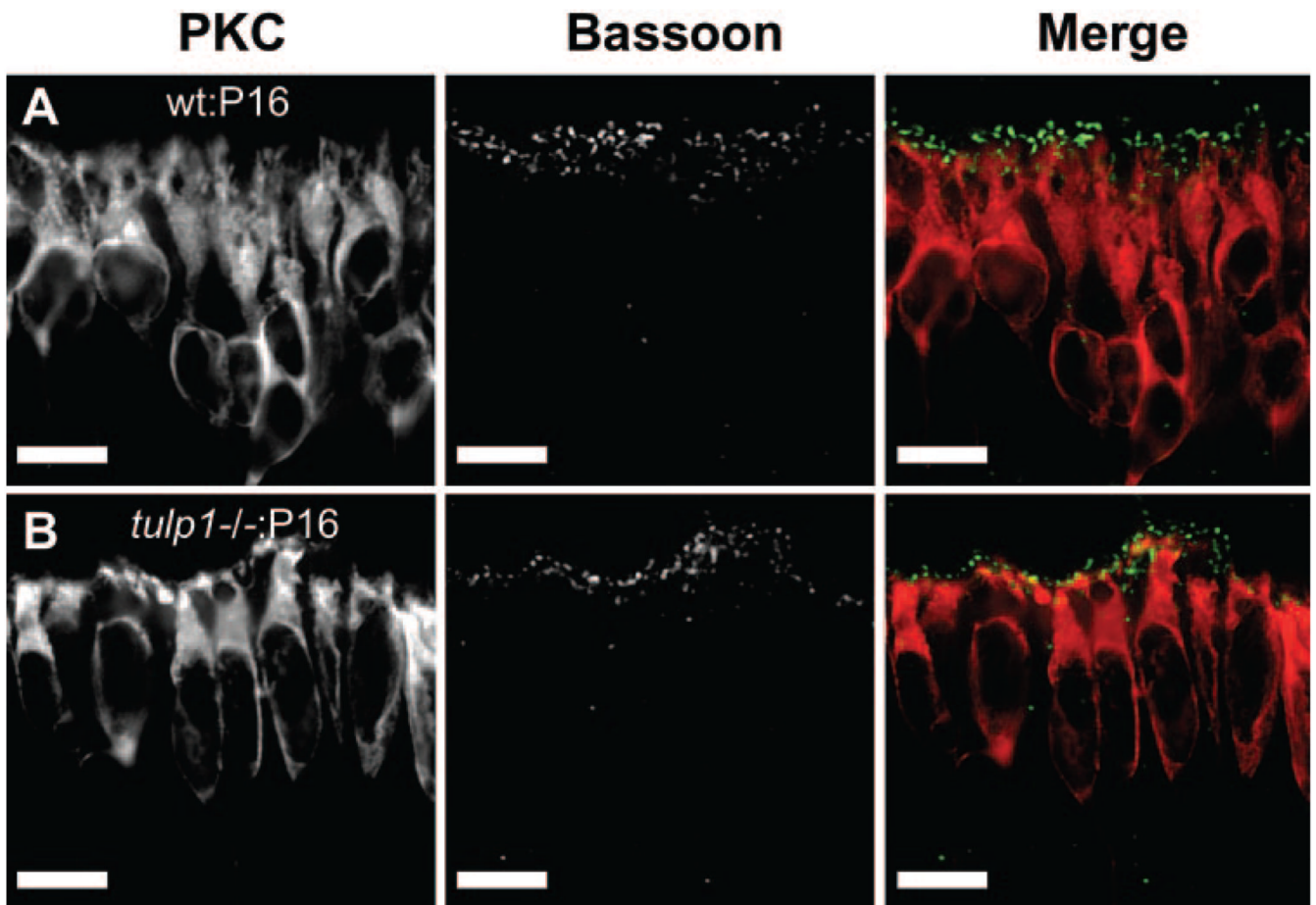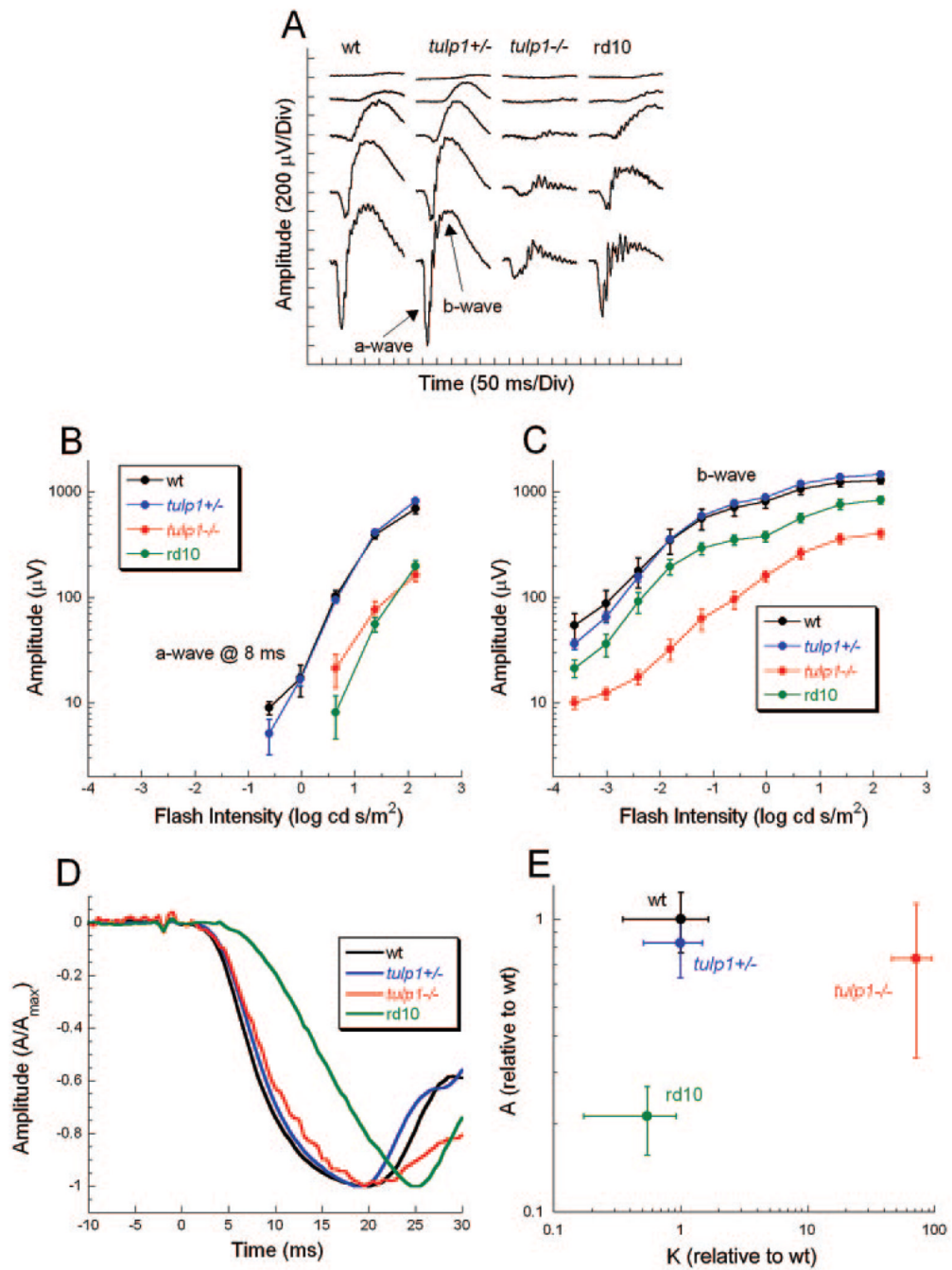
**FIGURE 7.**
Relationship between presynaptic and postsynaptic elements show deficits in the *tulp1*^{−/−}
retina. Deconvolution-generated images of immunofluorescence of PKC (*red*) and Bassoon
(*green*) in the OPL at P16 showing the relationship of the presynaptic and postsynaptic
elements. In the wt OPL (**A**), long and branching dendrites stretch toward the photoreceptor
terminals that are decorated with Bassoon-immunoreactive horseshoe-shaped ribbons. In the
*tulp1*^{−/−} OPL (**B**), dendrites show shortened appendages with reduced branching, and
Bassoon-immunoreactive ribbons appear punctate. However, the presynaptic and
postsynaptic elements are still closely apposed. Scale bars, 10 μm.

**FIGURE 8.**
Electroretinography of P16 mice. (**A**) Representative dark-adapted ERGs obtained from wt (*first column*), *tulp1*^{+/−} (*second column*), *tulp1*^{−/−} (*third column*), and rd10 (*fourth column*) mice. Intensity-response functions for the amplitude of the a-wave (**B**) and b-wave (**C**) of dark-adapted ERGs obtained from wt, *tulp1*^{+/−}, *tulp1*^{−/−} and rd10 mice. The amplitudes of the a- and b-waves are comparable in wt and *tulp1*^{+/−} mice, and are reduced in *tulp1*^{−/−} and rd10 animals. Note that the rd10 b-wave function is shifted downward, whereas the *tulp1*^{−/−} b-wave function appears shifted down and to the right. Data points indicate average ± SD for ≥5 mice. (**D**) Comparison of the leading edge of the dark-adapted ERG a-wave obtained to a high intensity stimulus for each genotype studied. In each case, the plot represents an

average of all mice tested, normalized to the a-wave trough. Note that normalized responses for wt, *tulp1*$^{+/-}$ and *tulp1*$^{-/-}$ mice overlap, whereas those of rd10 mice are delayed. (**E**) Comparison of *A* (equation 2) and *K* (equation 1) values obtained for each mutant genotype relative to the wt values. There is little difference in these parameters between wt and *tulp1*$^{+/-}$ mice. In comparison, rd10 mice have reduced values of *A* but not *K*, whereas *tulp1*$^{-/-}$ mice have increased values of *K* but not *A*.